Available online at www.sciencedirect.com

jmr&t Journal of Materials Research and Technology

journal homepage: www.elsevier.com/locate/jmrt

Original Article

Selective laser melting of Al–Si–10Mg alloy: microstructural studies and mechanical properties assessment

P. Ashwath [a], M. Anthony Xavior [b,*], Andre Batako [c], P. Jeyapandiarajan [b], J. Joel [b]

[a] Department of Engineering, University of Wales Trinity Saint David, Swansea, SA1 8PH, Wales, United Kingdom
[b] School of Mechanical Engineering, Vellore Institute of Technology, Vellore, 632014, Tamilnadu, India
[c] General Engineering Research Institute, LJMU, Liverpool, L3 5UX, United Kingdom

ARTICLE INFO

Article history:
Received 28 June 2021
Accepted 24 January 2022
Available online 7 February 2022

Keywords:
Additive manufacturing
Selective laser melting (SLM)
Aluminum alloys
Surface finish
Microhardness
Strength validation

ABSTRACT

Additive Manufacturing (AM) technique is widely recognized by aerospace sectors for its potential to fabricate complex shape components directly from a Computer-Aided Model data (CAM). Selective Laser Melting (SLM) is an innovative method high degree of adaptability among different AM techniques. SLM is one of the AM techniques adopted to produce the three-dimensional complex shape components. Current research work focuses on fabricating an Al–Si–10Mg aluminium alloy by SLM process which is studied for the influence of scanning speed and build orientation on the mechanical strength and surface finish of the as built component compared with as casted specimen. The importance of the sample studied for the scanning speed and built direction is relatively essential exclusively for dynamic applications. The as-built samples surface micrographs was surprisingly refined with a progressively reduced grain size diameter from 7.2 μm to 5.5 μm by increasing scanning speed compared to that of AlSi10Mg parts (~9.1 μm). The mean layer thickness increased from 20 μm to 30 μm by decreasing the scanning speed from 500 mm/s to 200 mm/s. Attractive advantage of the Orowan mechanism, fine grain strengthening, and the graded interfacial layer, a considerably-high microhardness (135 ± 3.1HV), and enhanced mechanical properties were achieved.

1. Introduction

Selective Laser Melting (SLM) is a progressive layer by layer additive manufacturing technique and is a cutting-edge method that unlocks the potential for digital additive manufacturing in various aerospace and space industries. Additive manufacturing by SLM is observed to be rapid, flexible, and cost efficient for complex components production from a computer aided design (CAD) model produced by any

* Corresponding author.
E-mail address: manthonyxavior@vit.ac.in (M.A. Xavior).
https://doi.org/10.1016/j.jmrt.2022.01.135

modeling platforms. Explicitly, most complex 3-dimensional design models with different geometries and shapes can be built with highest efficiency and automatically without involving additional milling path programs and post processing. Comparing with various AM techniques, SLM process is capable of producing components with good density and highest properties expected due to its rapid melting and solidification of the particles with ultra-fine-grained microstructure. Complex shape prototypes of the aerospace and space components can be manufactured in a short period and progress the quality of product design which facilitates the opening to review the faltering configurations [1]. Besides, AM inculcates distinct mode manufacturing of complex shape three-dimensional parts and diverse articulated structure, which could not be possible with conventional manufacturing methods, neglecting sub-assemblies of structural part members and assembling after post manufacturing. Distinct mode manufacturing by SLM techniques can significantly amend the way aerospace and space exploration complex parts that are newly built [2–4]. However, various researchers have studied on the complex parts that are directly manufactured and tested for microstructural and bulk characteristics of the additively manufactured components. There are numerous additive manufacturing techniques existing to manufacture aerospace-space exploration complex parts like 3D printing, stereolithography (SLA) and selective laser sintering (SLS). AM-manufactured space exploration complex parts found to be potential alternatives for many real time applications as they possess high strength, which are proficient to withstand and operate at both dynamic and static loading conditions [5]. Selective laser melting (SLM) a well-known AM method which is relatively demanding in recent years while manufacturing aerospace and space exploration complex shape ferrous and non-ferrous parts. SLM process is a cutting-edge manufacturing technology where various types of materials and different properties for explicit purpose are engineered to accomplish as per the application requirement in aerospace and space exploration industries [6–9]. AM manufacturing technique started in aerospace and space exploration application with fabricating complex shape plastic prototype composites at development stages and went on to the ferrous, non-ferrous and ceramic components. Selective laser melting (SLM) is used to manufacture the Al–Si–10Mg alloy plate which is tested for the tensile strength, micro hardness, surface roughness and microstructural analysis. SLM plate in both the vertical and horizontal built direction is tested to understand the influence of build orientation on the bulk strength and microstructural analysis of the manufactured part [10–12]. It is also important to study the microstructural resultant factor and surface finish of the as built part to understand the importance of employing secondary operations to reduce cost which play a significant role in AM techniques. Bulk properties, components service life and cost for production are the key important factors that control the choice of choosing a new additive technique to solve the modern demands in the aerospace and space exploration industries. The SLM technique has a direct or indirect influence of its own process parameters during complex components manufacturing. Other important factors like type of machine, laser source, laser power, layer thickness, hatch spacing, build orientation, scan speed, type of work piece, material used for manufacturing do have potential impact on the final product outcome after the SLM process. Some of the factors mentioned above are maintained constant in the current research and few changing parameters are used to process the specimens.

2. Experimentation and methodology

2.1. *Additive manufacturing by SLM process*

As displayed in Fig. 1(a), the 3D schematic of the SLM 280 2.0 Multi laser system supplied by SLM solutions Pvt Ltd., Bangalore, India which possess a string laser of emitting laser beam of average wavelength 1069 nm. The maximum power output of the laser is 100 W with a laser spot diameter of ~60 μm. The SLM experimental parameters are tabulated in Table 1. The substrate backing plates were preheated twice prior to starting the SLM process to ensure the scanning of the leaser and to improve the efficiency of the built specimen. S-cross lay hatching strategy was used to fabricate specimen

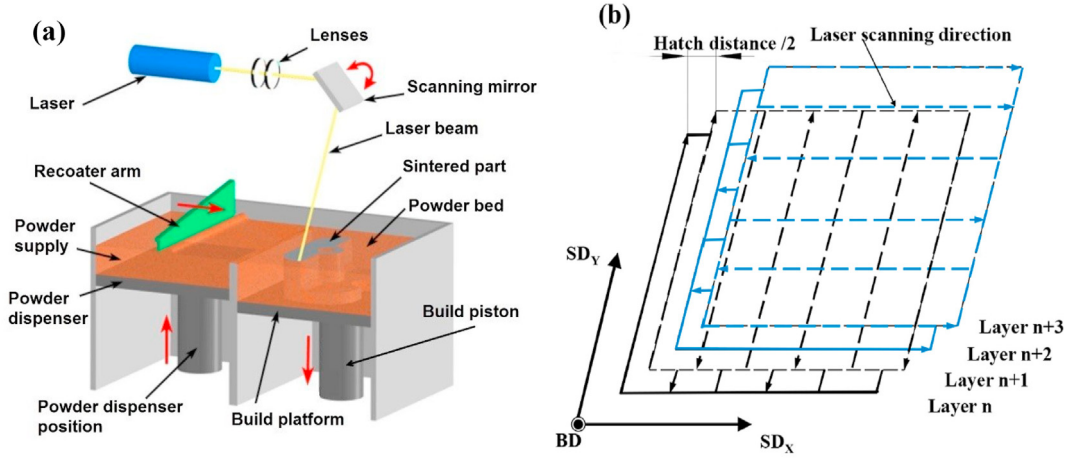

Fig. 1 – (a) Graphical representation of SLM rig and (b) Laser scanning strategy by S-Cross method.

Table 1 – Tensile data of as cast and SLM as built Al–Si–10Mg in XY and Z direction.

rocessing condition as built and built direction	Tensile Strength (MPa)		Yield Strength (MPa)		Modulus of elasticity (GPa)	
	Xy direction	Z direction	Xy direction	Z direction	Xy direction	Z direction
500 mm/s and 20 μm	360 ± 2.9	390 ± 2.1	283 ± 3.5	320 ± 2.3	70 ± 1.6	70 ± 1.5
200 mm/s and 30 μm	271 ± 3.3	325 ± 2.6	259 ± 1.9	305 ± 2.1	63 ± 1.3	63 ± 1.1
As casted tensile strength is 279 ± 1.9 MPa, Yield Strength is 235 ± 2.2 MPa and Modulus of elasticity is 57 ± 1.3 GPa.						

plate of 150 × 100 × 5 mm LxBxT plate under argon atmosphere and with oxygen content in the processing chamber below 50 ppm. As shown in Fig. 1(b), the built plate was scanned twice with bi-directional vectors in SD_x and scanned twice in direction of SD_y consecutively for attaining the build track homogeneity. The layer-by-layer hatching was performed at a hatching spacing of 150 μm. The layer thickness for performing SLM was 20 μm and 30 μm. The laser spot diameter was maintained at 100 μm.

2.2. Materials

Gas atomized powder of Al–Si–10Mg was obtained from Ampal Inc. USA with average particle size of 10 μm with 98.9% purity level. The as received powder was ball milled for 30 min at 600 rpm to ensure the powder surface with oxidation are removed completely in acetone medium and the powder mixture is dried in a vacuum microwave oven at 100 °C for 6 h. The dried powder is immediately transferred to the powder supply chamber of the SLM process rig. The particle size of the processed powder was validated by the Master size 3000 type particle analyzer as shown in Fig. 2(a). The powder is further studied for the composition by using hand held X-Sort X-ray fluorescence XRF analyzer as details of the composition shown in Fig. 2(b). Figure 2(c) shows the Scanning Electron Microscope image (SEM) of powder morphology exhibiting the shape of the powder were uniform and in near spherical in shapes.

2.3. Material characterization

Laser absorptive nature of the as received Al–Si–10Mg powder was studied using diffuse reflectance spectroscopy (DRS) technique. The measurement was attained by using a Lambda 900 spectrometer attached and integrated with a sphere of diameter 150 mm. The results were measured and validated with the wavelength ranging from 200 to 2000 nm. The plate that was as built were transferred carefully to a wire electric discharge machine to cut the samples into desired shape of tensile sample as per ASTM E08 and small 10 × 10 mm samples for microstructural, Hardness and SEM/Transmission Electron Microscopy (TEM) observations. The as cut samples were polished using grit papers with standard methods and etched with Keller's reagent (95 ml distilled water, 1 ml HF,1.5 ml HCl, 2.5 ml HNO_3) for 25s. Optical inverted microscope and high-resolution scanning electron microscope (HRSEM) was used to investigate the microstructural refinement of the as SLM built samples. For the validation on the grain size studies and orientation of the grains Electron Backscatte Diffraction (EBSD) method was used. Samples for EBSD were prepared by electro polishing with 20% perchloric acid and 80% methanol for 100 s at potential difference of 12 V. The EBSD analysis was performed using FEI-Quanta 200HR-SEM following step size of 0.1 μm and with TSL OIM software. FEI Technai 20 G2S-Twin High resolution transmission electron microscope (HRTEM) with 200 Kv capacities was used to analyze the microstructure mechanics at the SLM as built surface in terms of grain size, shape and nucleated precipitates. The HRTEM samples with size 0.5 mm thickness were taken from the area perpendicular to the built direction by using hand held diamond cutter. Further mechanically polished thin film of size 75 μm with punched disc of diameter 40 μm was extracted and subjected to twinjet electro polishing using 10% perchloric acid and 90% methanol. For each explicit parameter, experimental data were recorded from an average of 3–5 entries. The phase formation during the process was studied by x-ray diffraction (XRD, D8 Advance, Cu Kα), and the peak intensities were recorded in the 2θ-range between 20° and 90°. Vickers hardness measurements were recorded and calculated on the cross-section by a Matsuzawa MMT-X with micro diamond indenter with 100 g acting load and a loading duration of 15 s.

3. Results and discussion

3.1. Microstructural studies and relative density studies

Figure 3 shows the built morphology and relative density of the as-built Al–Si–10Mg specimens in z direction scanned for twice in bi-directional directions SD_x and SD_y. The relative density was experimented and determined using Archimedes principle, as described by equation (1) [13]:

$$\rho = \frac{M_a}{M_a - M_w} * \rho_w \quad (1)$$

Where, ρ is the bulk density of the as-built specimen, ρ_w is the distilled water density as this particular parameter is highly temperature dependent, M_a is mass of the as built specimen in air and M_w is the immersed mass of the as built specimen in distilled water. The theoretical density of the Al–Si–10Mg was calculated from the structure of crystalline solid route as shown in equation (2):

$$\rho = \frac{n\,A}{V_c N_A} \quad (2)$$

Where n is the number of atoms/unit cell, A is the atomic weight of Al–Si–10Mg, V_c is the volume of unit cell which is a^3 for cubic structure and N_A is Avogadro's number (i.e., 6.022×10^{23} atoms/mol) and was calculated theoretical

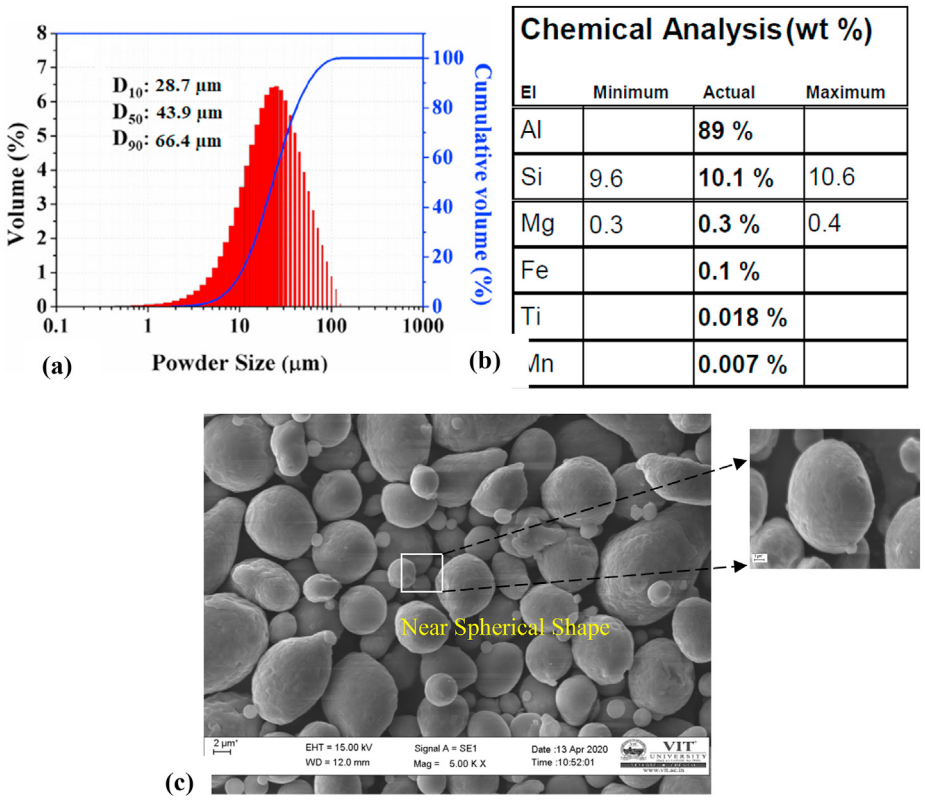

Fig. 2 – (a) Particle size distribution of Al–Si–10Mg processed powder, (b) XRF composition analysis report and (c) SEM image of Al–Si–10Mg processed powder.

density was found to be 2.59 g/cm^3, as also ascribed with the findings [14]. From Fig. 3 it is very clear that Al–Si–10Mg alloy had numerous keyhole pores and microstructural defects when fabricated through casting techniques and by employing additive manufacturing technique the alloy exhibited advantage in process ability by SLM method as shown in Fig. 3(c). However, the relative density of the casted Al–Si–10Mg was found to be 87.2% with noticeable keyholes and microstructural defects where as SLM processed specimen recorded with highest relative density of 94.7% free from micropores and macro pores (scan speed ~ 200 mm/s) [14]. There exists an inverse relation between the densification behavior and scanning speed of the process when fabricated by SLM technique. On reducing the induced energy input by increasing the scan speed to 500 mm/s, the as built plate exhibits prominent visible surface pores and micro cracks and recording a reduced relative density of 91.8%. Similar results were also reported by recent research where SLM processing at 600 mm/s scan speed produced a sample with lower relative density 93.8% and surface noticed with prominent visible micro pores, surface micro cracks, and keyholes with noticeable defects in the molten pool boundaries [14].

Significant property like laser reflectivity will determine the effectiveness of SLM process ability of Al–Si–10Mg alloy which was also reported in recent research [13–15]. This phenomenon means that proficient energy absorption of the alloy material for the same experimental parametric condition. Surprisingly, few volume percentages of unmelted alloy particles during the process could refill the pores formed on the surface of the plate during the stage of solidification, which eventually leads to improved relative density, this phenomenon is quite in adherence with recent research [16]. From Fig. 3(c), molten pool boundaries are noticed with large metallurgical pores which may be due to the gas trapped within the melt pool when scanned with 500 mm/s. Significant mechanism in the formation of large sized pores at the melt pool boundaries may be due to the inverse relation between the dynamic viscosity of the melt system with liquid flow temperature [2]. At 500 mm/s scanning speed, the molten pool temperature was observed to be restricted, which leads to higher dynamic viscosity of the alloy system with reduced flowability. This particular phenomenon leads to insufficient flow rate of the melt which eventually results in failure to fill the residual gaps leading to formation of large sized pores and keyholes [2,14–16]. Furthermore, at 500 mm/s scanning speed enhanced the capillary instability of the melt pool which resulted in splashing of tiny fluid droplets on the surface leading to micro pores and keyholes [16].

The XRD analysis data of the as casted and SLM processed as built specimens were studied and compared for 200 mm/s and 500 mm/s scanning speeds as shown in Fig. 4 (a) and (b). Element aluminium (Al) (JCPDS card 04–0787) and Silicon (Si) (JCPDS card 78–2500) were recorded as the significant compound phases in both as casted and SLM as built specimens with scanning speeds of 200 and 500 mm/s. The minor peak intensities related to the element magnesium (Mg) (JCPDS Card 22–0829) was recorded because of low Mg content. It is profound from the peak intensities that Al peak was recorded

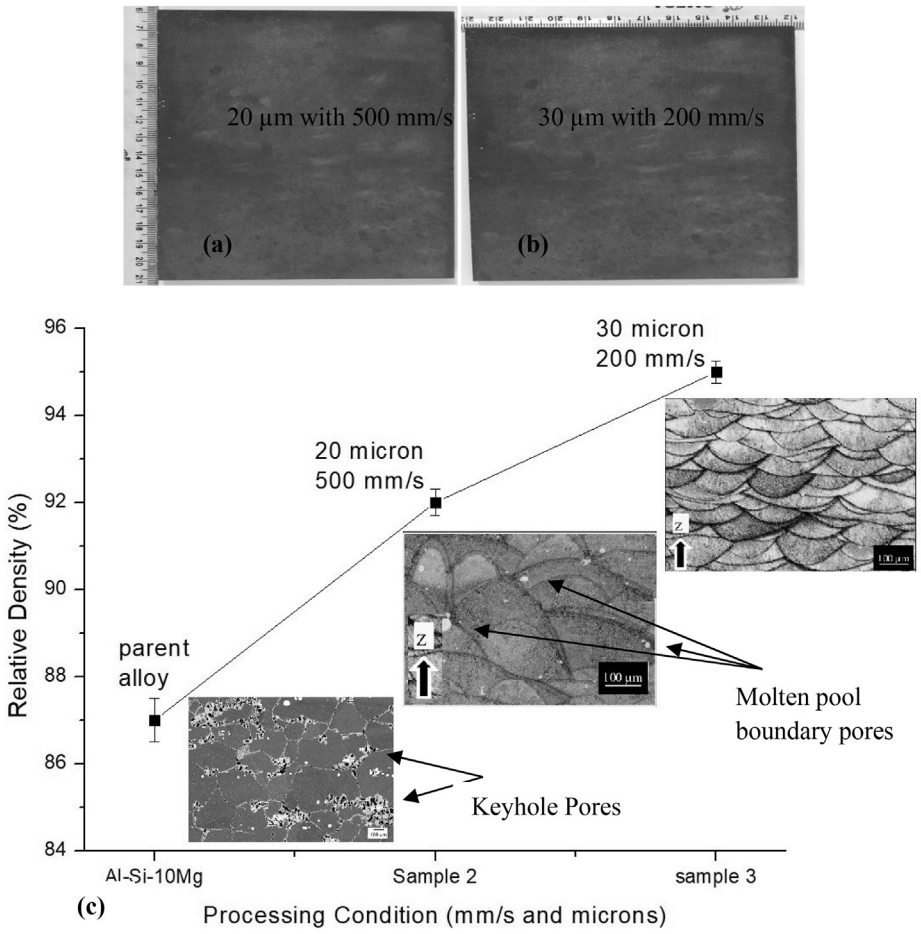

Fig. 3 – (a) (b) Al–Si–10Mg plate with dimension 150 × 100 × 5 mm LxBxT fabricated by SLM, (c) Relative density of as built specimen compared with the as casted Al–Si–10Mg specimens for two combinations of scanning speeds and layer thicknesses.

between 37° - 40° which shifted towards higher 2-theta angles with lowered scanning speed of 200 mm/s as shown in Fig. 4(b). This higher angle shift may be due to the factor of decreased lattice parameter, which may be majorly due to the lattice distortion induced by the formation of high dense melt pool experienced in the lower scanning speed of 200 mm/s [2,15,16]. Similar, research reported that higher Bragg angles shift of aluminium phases are due to the addition of external reinforcement particulates when processed with SLM which is in well correlation with the current findings. However, the

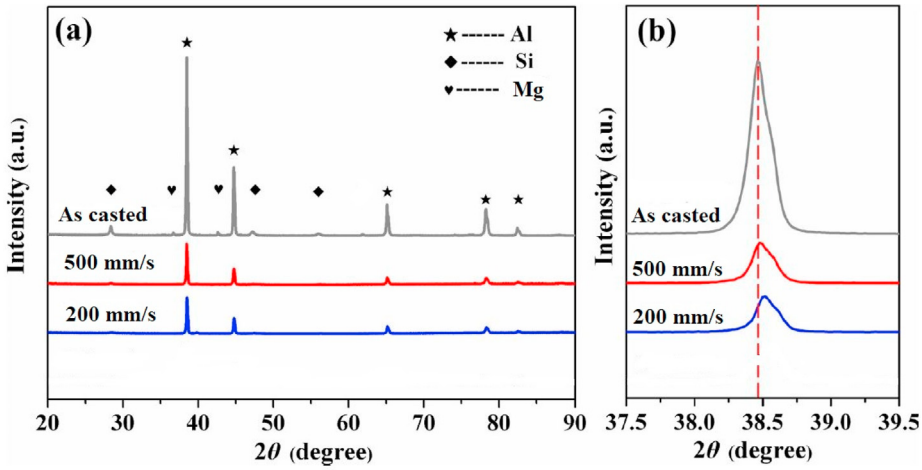

Fig. 4 – (a) XRD spectrum of as casted and SLM as built Al–Si–10Mg plate with 200 and 500 mm/s scanning speeds showing peak intensities in the range 2θ = 20° ~90° (b) smaller range peak intensities of 2θ = 37° ~ 40°.

influence of thermal stresses induced due to higher temperature gradient should also be considered.

Figure 5 represents the microstructure of the as casted and SLM as built Al–Si–10Mg specimens prepared by 200 mm/s and 500 mm/s. It is evident that melt pool clearly possesses fine grains zone with strong existence of equiaxed cellular microstructure comprised well distributed primary α-Al matrix combined with Si clusters which are fibrous in nature. The average grain size diameter (μm) was studied using Fei Quanta 3D FEG Focused Ion Beam (FIB) attached with an Energy Dispersive Spectroscopy (EDAX) equipment as shown in Fig. 5 (a-c). Considerable growth in grain size was noticed with decreasing scanning speeds from 500 mm/s to 200 mm/s, for the recorded average grain size diameter from 5.5 μm to 7.2 μm. It is evident that during SLM process, lower scanning speed induced relatively weak thermal gradient and diminished cooling rate, which failed to enhance refinement in grain microstructure in the as built specimen. In addition, duration of the melt pool always provided enough time for grain growth. It is worth noticing that SLM as built specimen exhibited fine grain size diameter characteristics way lesser than as casted samples (35 μm) (about 3 times reduction). Abundance of nucleated fibrous structured Si precipitate in the SLM as built specimen indicates that the certain quantity of fluid eutectic compounds tends to solidify resulting to form eutectic fibrous Si network along Al melt pool boundaries, normally on the degree of few nanometers of range 500–1400 nm [17–19].

High resolution TEM microstructure and phases formed as precipitates during the as-cast and SLM as built Al–Si–10Mg specimens are presented in Fig. 6. The HRTEM micrographs in Fig. 6(a) exhibits lamellar shaped precipitated phase with scale of 100 nm and it is observed to be consistently dispersed across the matrix. EDS validations of the precipitated particulates displays the element combinations of the as-cast specimen is more or less 72.71% of Al, 13.92% of Si, 1.12% of Mg and 10.43% of Fe, which is quite matching the β-Al5FeSi compound phase [20]. Figure 6(b) represents the HRTEM micrographs of the SLM as built Al–Si–10Mg, clearly exhibiting enriched eutectic Si elements along the melt pool boundaries containing α-Al cells. As per Fig. 6 (b) and (e) elements Fe and Mg were also segregated along with Si at the interlaced melt pool cell boundaries. The compositional nature of the Fe-bearing precipitates in the SLM as built specimens was more or less Al59.40Si.46Mg12Fe5.12, which is similar to the phase π-Al8Si6mg3Fe [21]. HAADF image in Fig. 6(b) shows that the melt pool cell boundary contains strongly bonded overlapped nano sized particles. And SAED pattern in the melt pool cell boundary is presented in Fig. 6(c), which clearly exhibits Si which poses ring like patterns and numerous discrete Al diffraction spots down the crystal orientation matching [2 0 0]. However, few tiny Si particles exhibits hexagonal shape precipitates that are in lined with

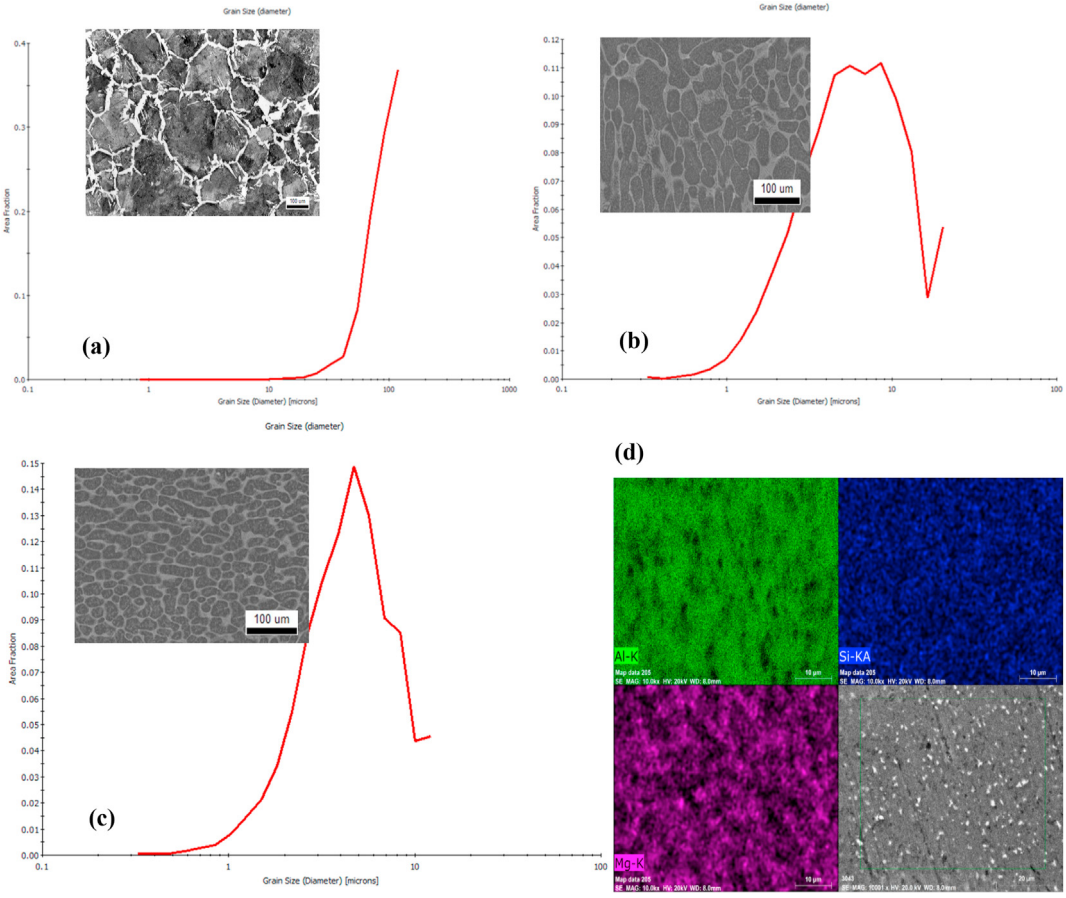

Fig. 5 – Microstructure and grain size diameter prediction by Electron Backscatter Diffraction (EBSD) method for Al–Si–10Mg (a) as casted, (b) SLM as built 200 mm/s, (c) SLM as built 500 mm/s and (d) EDS mapping analysis.

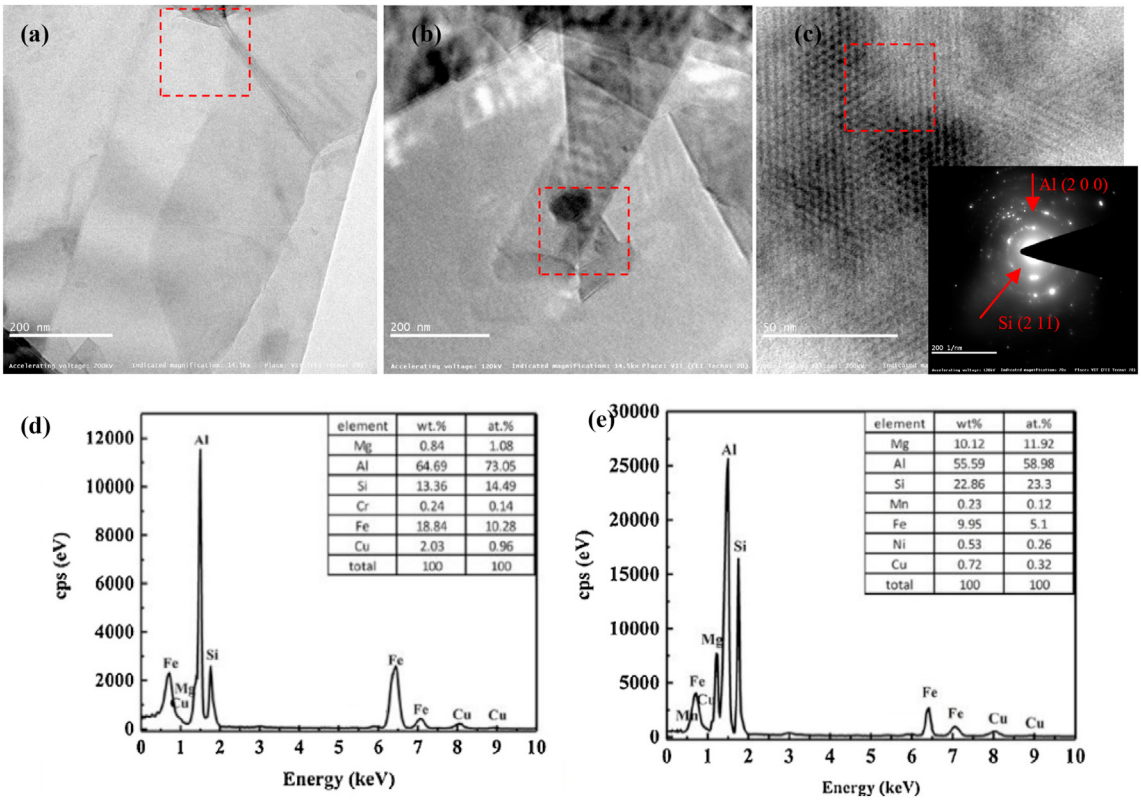

Fig. 6 – HRTEM HAADF image of (a) as casted, (b) SLM as built Al–Si–10Mg, (c) HRTEM corresponding to the melt pool boundaries and the corresponding selected area electron diffraction (SAED) pattern of the Al cell boundary and (d) (e) EDX elemental distribution of Al, Si, Mg and Fe within the square marked.

crystal orientation [2 1 1] matching π-Al8Si6Mg3Fe [21]. The microstructural difference and precipitate distribution in as cast specimen and SLM processes as built specimen are mainly due to two thermal theories dealing with solidification of liquid metal. For Al alloys rich in Si content, the dissolvability of fibrous Si is majorly influenced by the average melt temperature and this characteristic is considerably reduced with increase in temperature. As a result, Si particles are observed to dissolve in the aluminium matrix in the case of as casted specimen, where as in case of SLM as built samples most of the Si are found to be existed to form precipitate network structure around the Al melt pool cell boundary due to instant specific temperature. Various Fe-carrying intermetallic compounds are nucleated in both the as-cast and SLM as-built conditions which is driven by diverse cooling rates [22–24]. Due to the rapid cooling rates at 500 mm/s scanning speed during SLM process, most of the γ-Al phase were converted to form α-Al, which efficiently reduces the process of nucleation for Fe-carrying precipitates [23,25–28].

3.2. *Hardness and tensile properties*

As presented in Fig. 7(a), it is very clearly evident that scanning speed reduction from 500 mm/s to 200 mm/s leads to slight reduction in microhardness of the plate as built by SLM process in the Z direction. The SLM processes sample with scanning speed 200 mm/s recorded a microhardness value of 122 ± 4.4 HV, whereas the sample processed with scanning speed 500 mm/s recorded 135 ± 4.7 HV which is 14.8% greater compared to the as casted Al–Si–10Mg samples (109 ± 3.9 HV) as shown in Fig. 7(a). In general factors like processing condition, materials morphology, final grain size diameter, final relative density and the types and quantity of precipitates that are formed during the process are the ones that determine the mechanical properties of the final component. Acorrding to metallurgical science [14,19–22], there exist a linear relationship between the average grain size diameter D and microhardness of the metallic sample defined by the Hall–Petch relationship as given in equation (3):

$$H_v = H_0 + K_H D^{-½} \tag{3}$$

Where H0 and KH are constants that appropriate values. There exist a proportional relation between the Hv and the average grain size diameter $D^{-½}$, superior hardness values are achieved in the samples with fine grain size microstructure. Therefore at 500 mm/s scanning speed, the energy input reduced considerably, which tends to induce faster cooling rate as a result of which lower grain size diameters was achieved which is in good agreement with the fine grain strengthening mechanism [23] as evident from Fig. 5.

Besides, the Fe-carrying and Si-Carrying precipitates nucleated at the melt pool cell boundaries which are observed to be dispersed uniformly also play a key role in improving the microhardness of the SLM processed plate. This phenomenon is in good agreement with the dispersion strengthening mechanism (Figure 5 and Figure 6). However, the role of in-situ

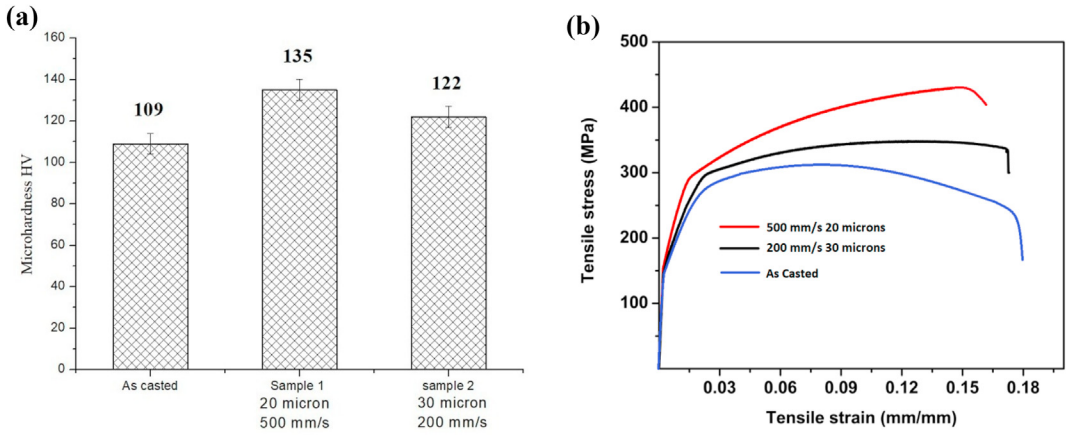

Fig. 7 – (a) Microhardness and (b) tensile stress–strain graph of as casted and SLM processed as built in Z direction of specimen with 500 m/s and 200 mm/s scanning speeds.

Si fibrous network at the melt pool cell boundaries should also be considered. This network not only played a significant role in improving the microhardness but also has strong ability to improve the interfacial bonding strength by combined effect of nucleating intermetallic precipitates within itself. The combined effects of fine grain strengthening mechanism and dispersion strengthening increased the microhardness of the SLM processed samples.

Figure 7(b) and Table 1 presents the tensile stress strain graphs and Tensile data of the as casted and SLM as built speimens tested in built direct Z and perpendicualar to built direct XY direction. Comparing earlier benchmark research results the current experimental data shows good concurrence in both as casted and SLM as built samples [2,14–19].

It seems that, the tensile strength and percentage of elongation of the as casted and SLM as built Al–Si–10Mg tested in z built direction and perpendicular to built direction (XY) were not identical. Comparing both as casted and SLM as built specimes, the SLM processed Al–Si–10Mg exhibits greater tensile strength in the built direction (Z) (390 ± 2.1 MPa) and in perpendicular direction (XY) (360 ± 2.9), where in as casted samples exhibited tensile strength of 279 ± 1.9 MPa at the better elongation as seen from Fig. 7(b). Comparing test data in the direction of Z and perpendicular to built direction (XY), Z direction tested samples recorded highest tensile strength with better elongation to failure in SLM processed as built samples. The elongation to failure in case of as casted and SLM as built samples are exhibiting closer rogimes showing no big difference in the values as shown in Fig. 7(b) and Table 1.

Considering anisotropy in tensile data of the current experimental specimens tested in Z direction, perpendicular to Z direction (XY) and SLM processing at 500 mm/s, 200 mm/s scanning speeds, HRSEM fracture studies are quite necessary to understand the failure mechanics when subjected to tensile loading of the as casted and SLM as built Al–Si–10Mg specimens. Figure 8 represents the fracture failure surface topography of the as-casted and SLM as built tested for Z direction tensile loading. Large dimple accumulations were noticed in the micro-fracture surface of the as casted Al–Si–10Mg in the casting Z direction which confirms the ductile mode of failure in the samples. This mode of failure in as casted samples lead to larger deformation to failure and highest elongation percentage as evident from Fig. 7(b). Irrespective of processing conditions (i.e. 500 mm/s and 200 mm/s) scanning speeds, the failure modes were also observed to be ductile modes. At 200 mm/s scanning speed built samples exhibited ductile failure leaving traces of medium sized dimples and holes, which is majorly due to the escaping Si-particles from the Al-matrix and escaping of the unmelted powder alloy particles from the interfaces of the matrix, oxide inclusions and pores already existing after the process Fig. 8(a), (b) and (c). However, at 500 mm/s scanning speeds the fracture surface exhibited tiny dimple shaped ductile failure as similar to earlier research results [19–23]. Considerable grain growth was noticed with the decrease in scanning speed from 500 mm/s to 200 mm/s, for the average grain diameter size from 5.5 μm to 7.2 μm. It is evident that during SLM process lower scanning speed induced relatively weak thermal gradient and weak cooling rate, which failed to enhance the grain refinement in the as built specimen.

Explicitly, in Al–Si–10Mg alloy the Si fibrous network and their brittle nature greatly influences the mechanical properties of the as casted or SLM as built specimens. As casted samples exhibited good elongation behavior as this phinomenon is mainly due to the major dissolved Si elements and nucleation of the Fe-carrying precipitates at the cell boundaries and in case of SLM as built samples the Si fibrous were quite controlling the ductile nature and the percentage of elongation. Because of fibrous nature of Si at the melt pool cell boundary, prevents the as built SLM samples to fail in ductile mode in larger extent as seen in Fig. 7(b) and also restricting the dislocation movements of the Al- matrix possessing ultra fine grain boundaries for 500 mm/s processed samples resulting in increased tensile strength. Fe-carrying and Si-carrying intermetallic precipitates which tends to poorly dissolve in the Al-matrix were found to be present in both the as-casted and SLM as built specimens. During the plastic deformation stage, strong stress concentration gradient was formed around the Fe-carrying and Si-carrying phases resulted in generation of microcracks and microvoids in both the as casted and as built SLM samples at 200 mm/s. In case of

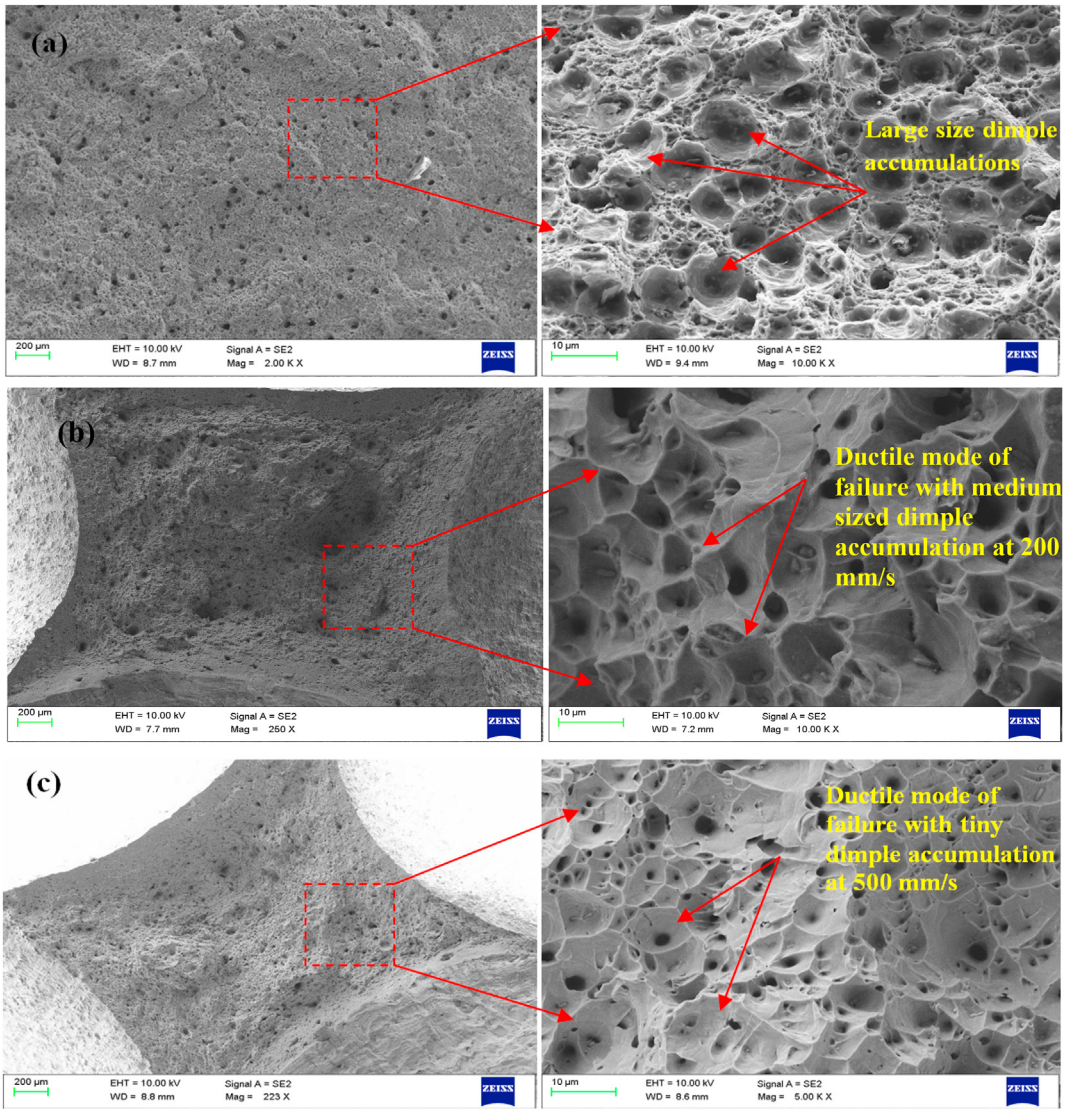

Fig. 8 – HRSEM images of fracture surfaces of (a) as-casted Al–Si–10Mg, (b) SLM as built tested in Z direction for 200 mm/s scanning speed and (c) SLM as built tested in Z direction for 500 mm/s scanning speed.

500 mm/s the intermetallic precipitate formation is mostly avoided by faster cooling rate which eventually ending up in displaying improved tensile and hardness values as seen in Table 1, Figure 7(b) and Figure 8(c).

4. Conclusion

This experimental research systematically investigated the microstructural improvement, mechanical behavior and the consequent process mechanisms of the as-casted and SLM as-built Al–Si–10Mg, including the nucleated precipitates, surface/matrix defects, fracture topography and failure mechanics. The following research findings are arrived from the current research work which are listed as follows.

1. Samples fabricated by SLM technique possesses a distinct microstructure compared to as casted samples. Intermetallic compound of β-Al-5Si–Fe lamellar shaped precipitate was observed to be homogeneously dispersed in as casted samples. Whereas, π-Al-8Si–6Mg–3Fe intermetallicprecipitate was found to be present at the melt pool cell boundary for the samples processed with 500 mm/s and 200 mm/s scanning speeds in SLM as built samples.
2. Having advantage of faster cooling rate at 500 mm/s during the SLM process, the effects like zener pinning and heterogeneous precipitate nucleation caused by intermetallics formation in the Al-matrix, leading to significant refinement in average grain size diameter from 7.2 μm to 5.5 μm as increasing the scanning speed from 200 mm/s to 500 mm/s.
3. Comparing as casted and SLM as built processes, SLM processes exhibited good microstrucural and strength integrity displaying enhanced hardness and tensile values compared to as casted Al–Si–10Mg samples.
4. The scanning speed during the SLM process displayed significant importance in deciding the final microstructural and strenght properties of the as buit specimen.

5. The combined effects of attaining ultra fine grain size, precipitate distribution, Si-carrying and Fe-carrying particles at the melt pool cell boundaries, and relative density greatly increased thehardness and tensile properties of the SLM additive manufactured plate.

Declaration of Competing Interest

The authors declare that they have no known competing financial interests or personal relationships that could have appeared to influence the work reported in this paper.

REFERENCES

[1] Croteau Joseph R, Griffiths Seth, Rossell Marta D, Leinenbach Christian, Kenel Christoph, Jansen Vincent, et al. Microstructure and mechanical properties of Al-Mg-Zr alloys processed by selective laser melting. Acta Mater 2018;153:35–44.

[2] Yan Qian, Song Bo, Shi Yusheng. Comparative study of performance comparison of AlSi10Mg alloy prepared by selective laser melting and casting. J Mater Sci Technol 2020;41:199–208.

[3] García-Moreno Francisco. Commercial applications of metal foams: their properties and production. Materials 2016;9(2):85.

[4] Trevisan Francesco, Calignano Flaviana, Lorusso Massimo, Pakkanen Jukka, Aversa Alberta, Paola Ambrosio Elisa, et al. "On the selective laser melting (SLM) of the AlSi10Mg alloy: process, microstructure, and mechanical properties. Materials 2017;10(1):76.

[5] Wu Jing, Wang XQ, Wang Wei, Attallah MM, Loretto MH. Microstructure and strength of selectively laser melted AlSi10Mg. Acta Mater 2016;117:311–20.

[6] Zhang Hu, Zhu Haihong, Qi Ting, Hu Zhiheng, Zeng Xiaoyan. Selective laser melting of high strength Al–Cu–Mg alloys: processing, microstructure and mechanical properties. Mater Sci Eng, A 2016;656:47–54.

[7] Fousova Michaela, Dvorsky Drahomir, Vronka Marek, Vojtech Dalibor, Lejcek Pavel. The use of selective laser melting to increase the performance of AlSi9Cu3Fe alloy. Materials 2018;11(10):1918.

[8] Calignano F. Design optimization of supports for overhanging structures in aluminum and titanium alloys by selective laser melting. Mater Des 2014;64:203–13.

[9] Li Ruidi, Wang Minbo, Yuan Tiechui, Song Bo, Chen Chao, Zhou Kechao, et al. Selective laser melting of a novel Sc and Zr modified Al-6.2 Mg alloy: processing, microstructure, and properties. Powder Technol 2017;319:117–28.

[10] Liu Yujing, Li Shujun, Hou Wentao, Wang Shaogang, Hao Yulin, Yang Rui, et al. Electron beam melted beta-type Ti–24Nb–4Zr–8Sn porous structures with high strength-to-modulus ratio. J Mater Sci Technol 2016;32(6):505–8.

[11] Liu YJ, Liu Z, Jiang Y, Wang GW, Yang Yang, Zhang LC. Gradient in microstructure and mechanical property of selective laser melted AlSi10Mg. J Alloys Compd 2018;735:1414–21.

[12] Read Noriko, Wang Wei, Essa Khamis, Attallah Moataz M. Selective laser melting of AlSi10Mg alloy: process optimisation and mechanical properties development. Mater Des 2015;65:417–24. 1980-2015.

[13] Prashanth KG, Shakur Shahabi H, Attar Hooyar, Srivastava VC, Ellendt N, Uhlenwinkel V, et al. Production of high strength Al85Nd8Ni5Co2 alloy by selective laser melting. Additive Manufac 2015;6:1–5.

[14] Spierings Adriaan B, Dawson Karl, Dumitraschkewitz Phillip, Pogatscher Stefan, Wegener Konrad. Microstructure characterization of SLM-processed Al-Mg-Sc-Zr alloy in the heat treated and HIPed condition. Additive Manufac 2018;20:173–81.

[15] Biffi CA, Fiocchi J, Tuissi A. Selective laser melting of AlSi10 Mg: influence of process parameters on Mg2Si precipitation and Si spheroidization. J Alloys Compd 2018;755:100–7.

[16] Gupta Munish Kumar, Kumar Singla Anil, Ji Hansong, Song Qinghua, Liu Zhanqiang, Cai Wentong, et al. Impact of layer rotation on micro-structure, grain size, surface integrity and mechanical behaviour of SLM Al-Si-10Mg alloy. J Mater Res Technol 2020;9(5):9506–22.

[17] Yu Wenhui, Leong Sing Swee, Chua Chee Kai, Tian Xuelei. Influence of re-melting on surface roughness and porosity of AlSi10Mg parts fabricated by selective laser melting. J Alloys Compd 2019;792:574–81.

[18] Yu Wen Hui, Leong Sing Swee, Chua Chee Kai, Kuo Che-Nan, Lei Tian Xue. Particle-reinforced metal matrix nanocomposites fabricated by selective laser melting: a state of the art review. Prog Mater Sci 2019;104:330–79.

[19] Marola Silvia, Manfredi Diego, Fiore Gianluca, Gabriele Poletti Marco, Lombardi Mariangela, Fino Paolo, et al. A comparison of Selective Laser Melting with bulk rapid solidification of AlSi10Mg alloy. J Alloys Compd 2018;742:271–9.

[20] Thijs Lore, Kempen Karolien, Kruth Jean-Pierre, Van Humbeeck Jan. Fine-structured aluminium products with controllable texture by selective laser melting of pre-alloyed AlSi10Mg powder. Acta Mater 2013;61(5):1809–19.

[21] Chen B, Moon SK, Yao X, Bi G, Shen J, Umeda J, et al. Strength and strain hardening of a selective laser melted AlSi10Mg alloy. Scripta Mater 2017;141:45–9.

[22] Kang Nan, Coddet Pierre, Lucas Dembinski, Liao Hanlin, Coddet Christian. Microstructure and strength analysis of eutectic Al-Si alloy in-situ manufactured using selective laser melting from elemental powder mixture. J Alloys Compd 2017;691:316–22.

[23] Kang Nan, Coddet Pierre, Liao Hanlin, Baur Tiphaine, Coddet Christian. Wear behavior and microstructure of hypereutectic Al-Si alloys prepared by selective laser melting. Appl Surf Sci 2016;378:142–9.

[24] Prashanth Konda G, Scudino Sergio, Chaubey Anil K, Löber Lukas, Wang Pei, Attar Hooyar, et al. Processing of Al–12Si–TNM composites by selective laser melting and evaluation of compressive and wear properties. J Mater Res 2016;31(1):55–65.

[25] Li XP, Wang XJ, Saunders Martin, Suvorova Alexandra, Zhang LC, Liu YJ, et al. A selective laser melting and solution heat treatment refined Al–12Si alloy with a controllable ultrafine eutectic microstructure and 25% tensile ductility. Acta Mater 2015;95:74–82.

[26] Yang Kun V, Paul Rometsch, Davies CHJ, Huang Aijun, Wu Xinhua. Effect of heat treatment on the microstructure and anisotropy in mechanical properties of A357 alloy produced by selective laser melting. Mater Des 2018;154:275–90.

[27] Zhang Jinliang, Song Bo, Wei Qingsong, Bourell Dave, Shi Yusheng. A review of selective laser melting of aluminum alloys: processing, microstructure, property and developing trends. J Mater Sci Technol 2019;35(2):270–84.

[28] Zhou Le, Mehta Abhishek, Schulz Esin, McWilliams Brandon, Cho Kyu, Sohn Yongho. Microstructure, precipitates and hardness of selectively laser melted AlSi10Mg alloy before and after heat treatment. Mater Char 2018;143:5–17.